

An observation-constrained estimation of brown carbon aerosol direct radiative effects

Yueyue Cheng^{1#}, Chao Liu^{1#}, Jiandong Wang^{1,*}, Jiaping Wang², Zhouyang Zhang¹, Li Chen¹, Dafeng Ge², Caijun Zhu², Jinbo Wang², and Aijun Ding²

5 ¹ Collaborative Innovation Center on Forecast and Evaluation of Meteorological Disasters/China Meteorological Administration Aerosol-Cloud-Precipitation Key Laboratory, School of Atmospheric Physics, Nanjing University of Information Science and Technology, Nanjing 210044, China

² Joint International Research Laboratory of Atmospheric and Earth System Sciences, School of Atmospheric Sciences, Nanjing University, Nanjing, 210023, China

10 *Correspondence to: Jiandong Wang (jiandong.wang@nuist.edu.cn)

These authors contributed equally: Yueyue Cheng, Chao Liu

Abstract. Brown carbon (BrC) is an organic carbon component with noticeable absorption in the ultraviolet and short visible wavelengths, which influences the global radiative balance. However, assessing BrC radiative effects remains a challenging task owing to the scarcity of direct BrC observations and the uncertainties regarding their chemical and optical properties. This

15 study proposes an efficient method for estimating BrC radiative effects based on the available observational data. The light-absorbing properties of BrC obtained from aethalometer measurements and an optical separation method were combined with simulated BrC optical properties to determine the mass concentrations. An optical closure study was conducted to constrain the total and other aerosol contents. Subsequently, we estimated the aerosol optical properties and concentrations. Such a state-of-the-art combination of measurements and numerical models provides primary variables for simulating radiative transfer to

20 estimate BrC radiative effects. We used observations conducted over four months (from July 1 to November 18, 2021) in Nanjing (a megacity in East China) as an example. During the observational period, BrC absorption constituted 8.7–34.1% of the total aerosol absorption at 370 nm. In the atmosphere, BrC plays a warming role, with its average instantaneous radiative

25 forcing (RF) and standard deviation of $4.0 \pm 2.3 \text{ W m}^{-2}$ corresponding to $15 \pm 4.2\%$ of the black carbon (BC) RF. At the surface, the BrC-induced actinic flux (AF) attenuation was comparable to that caused by BC, accounting for over 55% of the BC effects in the UV range and almost 20% in the visible range. The photosynthetically active radiation (PAR) attenuated by BrC was approximately $33.5 \pm 9.4\%$ of that attenuated by BC. Furthermore, we quantified the influences of several BC and BrC microphysical and optical properties on their radiative effects. These findings provide valuable insights for understanding BrC radiative effects; moreover, they highlight the importance of and necessity for improved observation and modeling of BrC properties.

30 1 Introduction

Carbonaceous aerosol is a major component of atmospheric aerosol that directly and indirectly influences the radiative budget of the Earth (Bond et al., 2006; Laskin et al., 2015). Carbonaceous aerosol includes organic carbon (OC) and black carbon (BC). Because of its strong light absorption in the visible and near-infrared regions, BC plays a crucial role as a climate warming agent (Moosmüller et al., 2011; Bond et al., 2013). Conversely, although OC is primarily thought to scatter aerosol 35 and cool the atmosphere, recent studies have indicated that a collection of OC compounds also possesses non-negligible light absorption (Alexander et al., 2008; Laskin et al., 2015). This subset of OC, also known as brown carbon (BrC), absorbs

ultraviolet (UV) and shortwave visible light, with its absorption diminishing as the wavelength increases (Chen and Bond, 2010; Kirchstetter and Thatcher, 2012). Therefore, BrC exhibits a significantly higher absorption Ångström exponent (AAE) than BC (Lack and Langridge, 2013; Mohr et al., 2013). Previous studies have shown that BrC could contribute up to 10% to 40 carbonaceous aerosol absorption at visible wavelengths and up to 20–50% at shorter wavelengths (Chen et al., 2020; Zhang et al., 2020; Pani et al., 2021). This substantial contribution leads to notable direct radiative effects (DREs) at the top of the atmosphere (TOA), with a global average value ranging from 0.1 to 0.6 $\text{W}\cdot\text{m}^{-2}$ (Feng et al., 2013; Huang et al., 2018; Jo et al., 2016; Kirillova et al., 2014). The DREs offset the cooling effects deriving from scattering-dominant aerosol to varying extents 45 (Liu et al., 2014; Zhang et al., 2017b, 2021b). Lin et al. (2014) reported that the BrC DREs could be 27% to 70% of those attributed to BC. Although BrC has recently attracted significant interest, our understanding of this carbonaceous component and its effects remains relatively limited, with significant uncertainties.

Currently, materials such as humic-like substances, polycyclic aromatic hydrocarbons, and lignin are all considered as BrC. Diversity in the chemical nature and microphysical properties of the BrC components introduces substantial variations in their 50 content and optical properties (Andreae and Gelencser, 2006). Even in well-controlled chamber experiments, BrC light absorption is influenced by various factors (Chen and Bond, 2010; Cai et al., 2020; Zhong and Jang, 2014; Liu et al., 2016), such as combustion conditions (e.g., burning temperature), atmospheric acidity, NO_x concentrations, and relative humidity. Liu et al. (2019) measured the optical properties of atmospheric water-soluble BrC in eastern China and reported BrC absorption coefficients of 9.4 Mm^{-1} at a wavelength of 365 nm, i.e., much smaller than those observed in Beijing (14.0 Mm^{-1}) 55 or Xi'an (19.6 Mm^{-1}) (Yan et al., 2015; Li et al., 2020). Choudhary et al. (2021) investigated BrC deriving from the burning of paddy and wheat residues in the source region of the Indo-Gangetic Plain, obtaining absorption coefficients at 405 nm of 134.8 Mm^{-1} and 47.1 Mm^{-1} , respectively. Paraskevopoulou et al. (2023) indicated that BrC absorption coefficients under intense residential wood burning conditions in Southeastern Europe could vary by a factor of 1.6 because of solvent differences. These results confirm that significant uncertainties regarding BrC chemicals and their optical properties remain.

60 Considerable attention has been devoted to estimating the global radiative effects of BrC by using numerical models (Feng et al., 2013; Wang et al., 2014, 2018b). These simulations mostly assume that a specific fraction of organic aerosol is BrC and use the measured minimum or maximum BrC absorption properties to perform radiative parameterization (Feng et al., 2013; Lin et al., 2014). For instance, Feng et al. (2013) assumed that 66% of primary organic aerosol from biofuels or biomass are 65 BrC and absorptive, whereas Lin et al. (2014) assumed that all primary organic aerosol from biofuel and biomass sources are BrC, as well as secondary organic aerosol produced by biogenic and anthropogenic emissions. Chemical transport and radiative transfer models have been used to simulate global or regional distributions of BrC, and to quantify its radiative effects, both of which show significant differences, primarily because of limited constraints on BrC properties (Jo et al., 2016; Wang et al., 2014; Yan et al., 2018). However, direct large-scale and long-term observations of BrC are scarce. Zeng et al. (2020) addressed 70 this issue by estimating the BrC DRE based on direct BrC observations collected from aircraft flights near pole-to-pole latitudes.

These authors discovered that BrC absorption contributes 7 to 48% of the TOA clear-sky instantaneous forcing by all absorptive carbonaceous aerosol. Although this methodology has significant potential, such direct atmospheric BrC observations are not sufficient (Saleh, 2020).

75 In summary, current BrC DRE estimations are based either on numerical modeling predictions based on specific assumptions or well-planned and equipped field campaign measurements. Given the scarcity of and challenges associated with *in situ* BrC observations, the current study proposed a simplified but observation-constrained model to quantify BrC radiative effects. Radiative forcing (RF, only direct radiative forcing) and influences on the photosynthetically active radiation (PAR) and actinic flux (AF) were considered and discussed. To reach this objective, we combined the readily available atmospheric and aerosol 80 observations and fundamental numerical optical simulations, and we used observations conducted over four months in Nanjing as an example for evaluating BrC radiative effects relative to those of BC.

2 Sampling sites and observations

This study provides a general observation-constrained method for estimating BrC radiative effects by utilizing easily accessible conventional observations. First, aerosol properties from ground-based measurements were obtained, including light 85 absorption coefficients (*Abs*, in a unit of Mm^{-1}) from a multi-wavelength aethalometer, light scattering coefficients (*Sca*, in a unit of Mm^{-1}) from a nephelometer, retrieved aerosol optical depth (*AOD*) from a Sun-photometer and the PM_{10} mass concentration ($M_{\text{PM}_{10}}$, in a unit of $\mu\text{g m}^{-3}$) from an aerosol particle size distribution sampler. A multi-wavelength aethalometer 90 (Model AE-33, Magee Scientific Corporation, California, USA) with a time resolution of 5 min continuously measured the aerosol *Abs* at wavelengths of 370, 470, 520, 590, 660, 880, and 950 nm. The light absorption coefficients were obtained from the measured attenuation coefficients Abs_{ATN} by correcting the effects deriving from filter loading and multiple scattering 95 using Eq. (1) (Schmid et al., 2006):

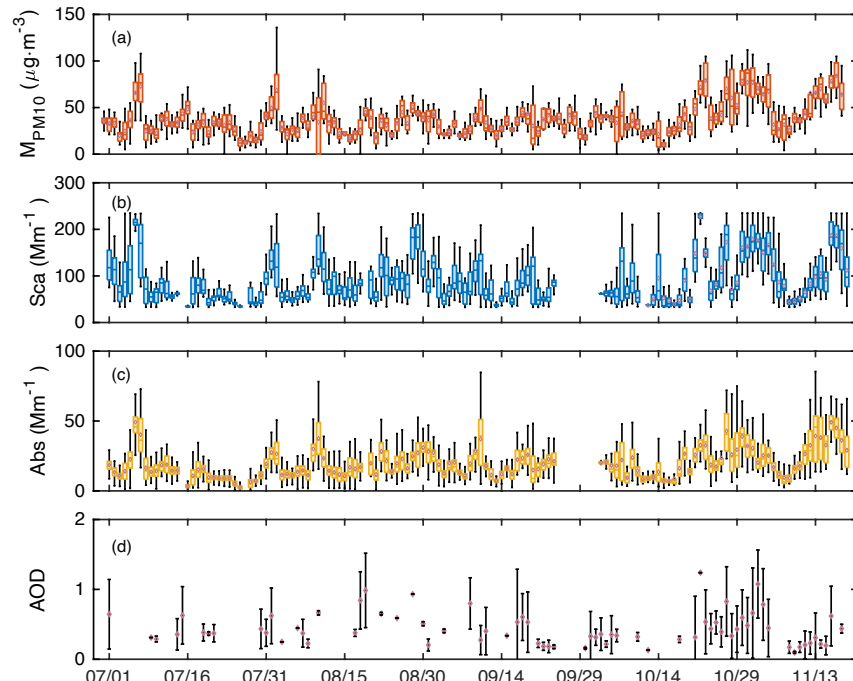
$$\text{Abs}_\lambda = \frac{\text{Abs}_{\text{ATN}}}{(C_{\text{ref}} + C_{\text{scat}})^R}, \quad (1)$$

where R is the function for filter-loading correction, and C_{ref} is the multiple scattering correction factor (set to 4.26) following Coen et al. (2010). C_{scat} represents the aerosol scattering correction, which is calculated using the *Sca* and scattering 95 Ångström exponents at three wavelengths (450, 525, and 635 nm) obtained from an integrating nephelometer (AuroraTM 3000, Ecotech, Australia) following Arnott et al. (2005). The measured *Sca* values with a time resolution of 1 min were adjusted for hygroscopic growth when $RH > 50\%$ (Zhang et al., 2015). A Sun/sky radiometer (CE318-T Photometer, CIMEL Electronique, France) was employed to obtain the retrieved *AOD* from ultraviolet to near-infrared wavelengths centered at 440, 500, 670, 870, and 940 nm.

Nanjing, a megacity located in the Yangtze River Delta (YRD) region of China, is characterized by rapid growth and a dense population (Ding et al., 2013). Recent observational studies revealed the non-negligible light absorption of BrC in Nanjing and its remarkable influence on climate change. The aethalometer, nephelometer, and Sun/sky radiometer observations were conducted at the SORPES station ($118^{\circ}57'10''$ E and $32^{\circ}07'14''$ N), located at the Xianlin campus of Nanjing University in the western suburbs region, which is impacted heavily by human activity (Ding et al., 2013, 2016; Wang et al., 2018a). The M_{PM10} were obtained from the China National Urban Air Quality Real-time Publishing Platform (<http://113.108.142.147:20035/emcpublish/>), and hourly results were adopted at the closest national monitoring station to the SORPES (Xianlin University Town, $118^{\circ}54'45''$ E and $32^{\circ}06'10''$ N). The sampling period was from 1 June 2021 to November 18, 2021 (local time).

110

Figure 1 shows the temporal variations in the major parameters during the observational period, including M_{PM10} , Abs , Sca , and AOD . These observations were employed to determine the BrC concentrations and optical properties. As shown in Fig. 1, the statistical observations describe different aerosol properties. Note that AOD characterizes the accumulated aerosol extinction of the column, and the other variables represent the aerosol properties at the surface. The hourly mean M_{PM10} values are shown in Fig. 1(a), with daily mean values varying from 10 to 80 $\mu\text{g m}^{-3}$. The Abs and Sca reveal the ability of aerosol to absorb and scatter light, with daily mean values varying from 38 to 228 Mm^{-1} at 525 nm and from 4 to 52 Mm^{-1} at 520 nm, respectively. The AOD describe the aerosol attenuation effects on light, with daily mean values varying from 0.1 to 1.2 at 520 nm.



120

Figure 1. Time series of (a) PM_{10} , (b) Sca at 525 nm, (c) Abs and (d) AOD at 520 nm during the observations. The boxes in (a), (b), and (c) indicate the 25% and 75% quantile of daily observation data, and the tentacle whiskers indicate 5% and 95%. The line near the middle of each box indicates the median of the sample, and the red diamond symbol in the box indicates the mean value of the data within a day.

125 3. Extraction of BrC and non-BrC aerosol properties

The observations discussed above were used to constrain the background aerosol properties and distinguish BrC and BC components. To evaluate the radiative effects of BrC in the atmosphere, a combination of observations and well-accepted microphysical and optical characteristics were adopted (Fig. 2). First, aerosol properties, including $M_{PM_{10}}$, Abs , Sca , and AOD were obtained from direct observations corresponding to the red part of Fig. 2. The mass absorption cross section (MAC), 130 mass extinction cross section (MEC), single scattering albedo (SSA), and asymmetry factor (ASY) for each aerosol type derived from the modeled aerosol optical properties, which are illustrated in green (Fig. 2). The measured and simulated aerosol properties were combined using an optical closure study to partition the various aerosol properties, namely AOD , ASY, and SSA. With the derived aerosol properties, the radiative transfer model (Library for Radiative Transfer Model, LibRadTran Model) could be used to determine the BrC radiative effects and their contributions to the relative carbonaceous aerosol effects.

135

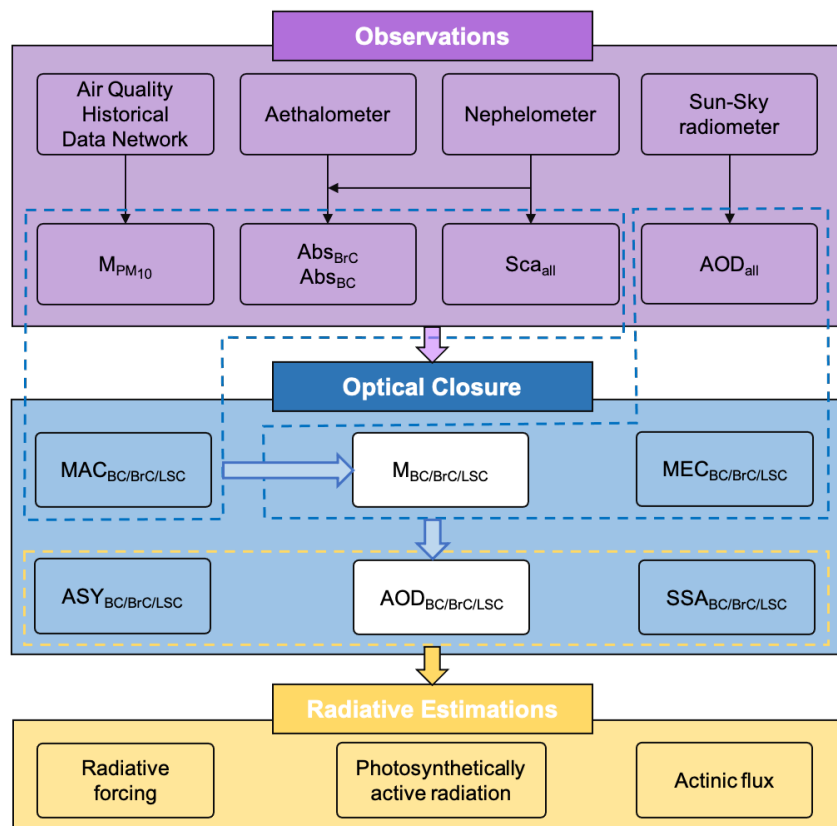


Figure 2. Flowchart of estimation of BrC radiative effect. The part with purple background corresponds to the direct observations used, which are detailed in Sections 2 and 3.1. The optical closure part, which uses the direct observations to separate the properties of each type of aerosol (i.e., AOD, SSA, ASY, surrounded by the yellow dotted line), is illustrated by the part with blue background. The bottom yellow part indicates the output for radiative estimations. We adopted a three-component aerosol model (BrC, BC, and pure light-scattering components, i.e., LSC). More details are available in Section 3.2. After clarifying the properties of each type of aerosol (i.e., AOD, SSA, ASY), the LibRadTran Model is used to estimate the BC and BrC radiative effects.

3.1 Extraction of BrC absorption

The optical properties of BrC, particularly absorption, are pivotal factors for estimating radiative forcing (Lu et al., 2015; Saleh et al., 2015). Initially, we extracted the absorptions of BC and BrC from the AE-33 observations following the absorption Ångström exponent (*AAE*) segregation method (Lack and Langridge, 2013; Mohr et al., 2013; Shen et al., 2017), which considers the distinct absorption spectral dependence of BC and BrC. Simplistically, the *AAE* deriving from the AE-33 measurements can be conceptualized as the average of BC and BrC absorption, in the form

$$AAE = \frac{-\ln(\frac{Abs_{\lambda_1}}{Abs_{\lambda_2}})}{\ln(\frac{\lambda_1}{\lambda_2})}. \quad (2)$$

By assuming that the absorption at longer wavelengths (880 nm was specifically considered here) is attributed solely to BC (Virkkula et al., 2015) and a constant BC *AAE* of 1 (i.e., $AAE_{BC} = 1$) (Lack and Cappa, 2010; Liakakou et al., 2020; Kaskaoutis et al., 2021; Zhang et al., 2021a), BC absorption at shorter wavelengths (Abs_{λ_BC}) can be derived at 880 nm (Abs_{880_BC} , which equals Abs_{880} directly from AE-33), as follows:

$$Abs_{\lambda_BC} = Abs_{880} \times \left(\frac{880}{\lambda}\right)^{AAE_{BC}}. \quad (3)$$

Then, the BrC absorption coefficients (Abs_{λ_BrC}) are obtained as the result of the absorption coefficients measured by the aethalometer (Abs_{λ}) minus the light absorption coefficients of BC (Abs_{λ_BC}), at a reference wavelength (λ):

$$Abs_{\lambda_BrC} = Abs_{\lambda} - Abs_{\lambda_BC}. \quad (4)$$

Following this segregation, Fig. 3 shows the time series of the daily average absorption coefficients of BrC and BC at 370 nm (Abs_{370_BrC} and Abs_{370_BC}) during the observation period, along with the fraction of BrC absorption to total aerosol absorption (P_{370}) at the same wavelength. The daily mean Abs_{370_BrC} varied from 1.1 to 13.0 Mm^{-1} , with a mean value of 4.4 Mm^{-1} , which falls in the same order of magnitude but is lower than that reported in Beijing (Du et al., 2014; Yan et al., 2015; Cheng et al., 2016) and Xi'an (Yuan et al., 2016a; Zhu et al., 2021). The variation of BrC absorption was similar to that exhibited by BC at shorter wavelengths. Abs_{370_BrC} showed slight seasonal variations, with a higher average value in autumn (4.9 Mm^{-1}) than in summer (2.8 Mm^{-1}).

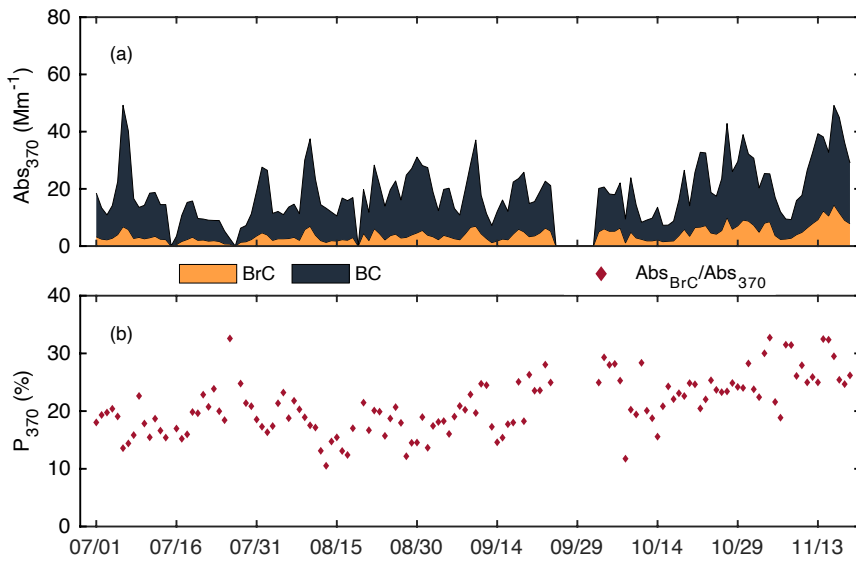


Figure 3. Variations of daily average (a) $Abs_{370,BC}$ and $Abs_{370,BrC}$ and (b) P_{370} during the measured period.

170 Overall, BrC aerosol accounted for 8.7 to 34.1% of the total carbonaceous aerosol absorption at 370 nm, which was similar to the monthly mean fractions from eight sites reported by Wang et al. (2016). The mean P_{370} in summer and autumn were 16 and 23%, respectively. The P_{370} in summer was lower than that reported in Xi'an (23.8%), but higher than the 11.7% reported in the Pearl River Delta region (Yuan et al., 2016a; Shen et al., 2017). The P_{370} tends to be higher in more polluted urban areas, such as Xianghe (China) and Mexico City, which has BrC absorption fractions of 30 to 40% at 400 nm (Barnard et al., 2008; 175 Yang et al., 2009). Compared with the results obtained by Wang et al. (2018) in Nanjing (mean $Abs_{370,BrC}$ and P_{370} of 5.9 Mm⁻¹ and 19.6% in summer, respectively), our data showed lower $Abs_{370,BrC}$ and higher $P_{370,BrC}$. Almost all P_{370} could reach percentages up to 20% in October and November, which should be considered when the subsequent radiative effects are estimated.

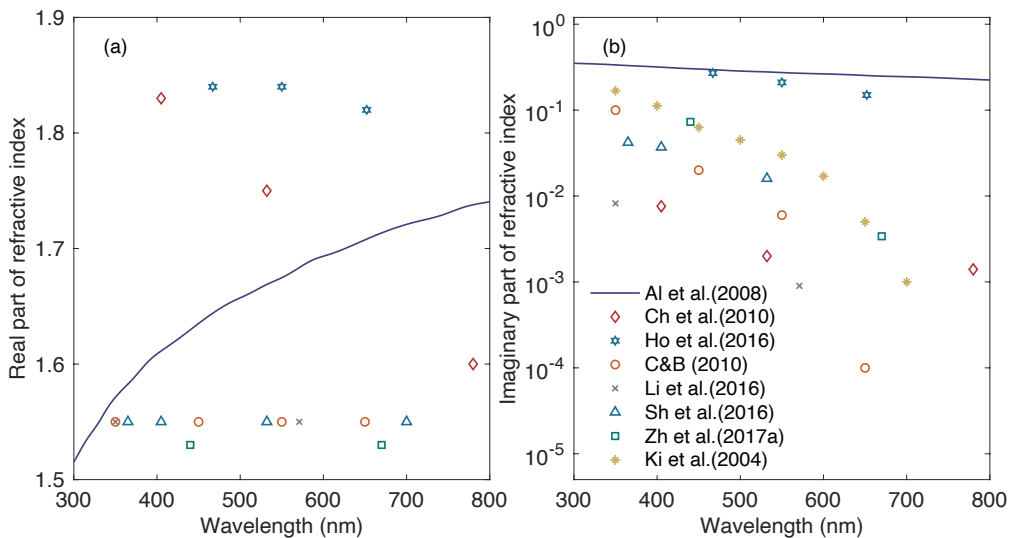
3.2 Aerosol optical properties

180 Although the conventional *in situ* measurements provided some of the overall aerosol optical properties and contents, that is, mass concentration (M), AOD , Abs , and Sca , those of each aerosol component are required to investigate their corresponding contributions. We assigned the known total aerosol properties to BrC using the above parameters in conjunction with an optical closure study. First, aerosol light absorption was assumed to be attributed solely to absorptive carbonaceous aerosol (BC and BrC) because the dust contribution was much less in Nanjing over the study period (Feng et al., 2023). Second, in addition to 185 BrC and BC, the remaining scattering-dominant aerosol (e.g., mainly sulfate and nitrate at our observation site) possessed similar optical properties and were, therefore, treated together as a non-absorbing type. Accordingly, we adopted a three-component aerosol model (BrC, BC, and pure light-scattering components, i.e., LSC) that was assumed to be externally mixed

(Yuan et al., 2016b). The absorption characteristics of BrC and BC were determined based on the observations described in Section 3.1, and their mass concentrations were calculated using Mie numerical simulations (Bohren and Huffman, 1983).

190

The BrC size distribution reported by Kirchstetter et al. (2004) was adopted in the Mie numerical simulations, i.e., a lognormal size distribution with a mean radius of 80 nm and standard deviation of 1.4. The density of BrC was set to $1.2 \text{ g} \cdot \text{cm}^{-3}$ (Lin et al., 2014). The real part of the BrC refractive index (RI) was set to 1.55, based on Chen and Bond (2010). However, the reported BrC RI imaginary part (k_{BrC}) exhibited a sharp increase toward shorter wavelengths, with different studies obtaining significant differences (Andreae and Gelencser, 2006). Figure 4 shows the BrC RI at wavelengths between 300 and 800 nm, retrieved from either *in situ* or laboratory observations (Alexander et al., 2008; Chakrabarty et al., 2010; Chen and Bond, 2010; Kirchstetter and Thatcher, 2012; Hoffer et al., 2016; Liu et al., 2016; Shamjad et al., 2016; Zhang et al., 2017a). The k_{BrC} values of Alexander et al. (2008) and Chakrabarty et al. (2010) are for individual amorphous carbon spheres produced from East Asia–Pacific outflow and chamber studies, respectively. Liu et al. (2016) obtained the k_{BrC} during a biomass-burning event in Colorado, USA, and Shamjad et al. (2016) sampled atmospheric BrC from Kanpur, India. The k_{BrC} in Kanpur (average k_{BrC} of 0.037) was found to absorb fourfold more at a wavelength of 405 nm than that in the USA (average k_{BrC} value of 0.009). Among the k_{BrC} , the group reported by Shamjad et al. (2016) was considered to have moderate values. Overall, the uncertainty of the real part of the BrC RI was less than that of the imaginary parts, showing differences of over an order of magnitude. Therefore, selecting a suitable set of RI is crucial to represent the optical properties of BrC, which significantly influenced our optical closure. To better restore the real situation of BrC in the atmosphere, we adopted the k_{BrC} linearly extrapolated from the investigation by Shamjad et al. (2016) in an urban Indian city, Kanpur (i.e., 0.041i at 370 nm, 0.026i at 470 nm, 0.018i at 520 nm, 0.0105i at 590 nm, and 0.004i at 660 nm).



210 **Figure 4. Real (a) and imaginary parts (b) of the BrC aerosol RIs. The sample case of Chen and Bond (2010) shown here is for methanol-soluble OAK_L_360 emitted from solid fuel pyrolysis. We derived the k_{BrC} based on $\frac{\rho\lambda\sigma}{4\pi}$, where ρ is the density of BrC, 1.65 g·cm⁻³. The legend is abbreviated as a combination of the first two letters of the first author's name and the year each study was published.**

215 We utilized the BC and sulfate (scattering-dominant) size distributions (with mean radiiuses of 35 and 69.5 nm and standard deviations of 1.7 and 2.03, respectively) from the Optical Properties of Aerosols and Clouds (OPAC) database (Hess et al., 1998; Chen et al., 2023). The densities of BC and scattering aerosol were assumed at 1.8 and 1.7 g·cm⁻³, respectively. The RIs of BC and sulfate aerosol at 550 nm were reported as 1.80–0.54i and 1.50–10⁻⁷i (Cheng et al., 2006; Ma et al., 2011; Yuan et al., 2016b), respectively, with minimal variation of the imaginary part of RI across wavelengths. Subsequently, the Mie theory 220 was applied to obtain the average optical properties of BrC, BC, and the pure-scattering components, respectively, which included their MAC, MEC, SSA, and ASY under the assumption of homogeneous spherical particles.

Based on the segregated *Abs* of light absorptive carbon aerosol (LAC, i.e., BC and BrC) in Section 3.1 and the simulated optical properties in Section 3.2, the mass concentration of BrC (M_{BrC}) can be estimated as

225
$$M_{BrC} = \frac{Abs_{\lambda, BrC}}{MAC_{\lambda, BrC}}, \quad (5)$$

where λ is set to be 520 nm unless indicated otherwise. M_{BC} can be given the same values as the corresponding values for the BC. This study assumed that the mass concentration of PM_{10} is the sum of all aerosol mass concentrations; therefore, the mass concentration of pure light-scattering aerosol (M_{LSC}) can be determined using Eq. (6).

$$M_{LSC} = M_{PM_{10}} - M_{BrC} - M_{BC}. \quad (6)$$

230 Thus far, the M values of all aerosol species on the surface have been obtained. Daily *AOD* observations were used to determine the mass concentration distributions in the vertical direction. A uniformly distributed and constant aerosol concentration was assumed for all layers within the height of the aerosol boundary layer (H) (Yan et al., 2015). Given that AOD_{All} was measured by a Sun-sky radiometer under actual atmospheric background, where the absorption by light-absorbing particles could be enhanced because of water uptake during the aging process, a factor of hygroscopicity (Kappa factor, f) 235 corresponding to atmospheric relative humidity was implemented to account for the enhancement (Kirillova et al., 2014). The H is given by Eq. (7):

$$H = \frac{AOD_{All}}{f \times (M_{BC} \times MEC_{BC} + M_{BrC} \times MEC_{BrC} + M_{LSC} \times MEC_{LSC})}, \quad (7)$$

where AOD_{All} and $MECs$ are from 520 nm. The H and M values of BC, BrC, and LSC are shown in Fig. 5. The H has mean values of 2.4 and 1.4 km during the summer and autumn, respectively. Higher aerosol boundary heights during summer create 240 favorable conditions for aerosol diffusion. Slight seasonal fluctuations occurred in M_{BC} , with average values of 2.6 and 3.1 $\mu\text{g}\cdot\text{m}^{-3}$ recorded during the summer and autumn, respectively. Conversely, M_{BrC} exhibited a relatively higher difference between seasons, with average values of 2.2 and 3.4 $\mu\text{g}\cdot\text{m}^{-3}$ observed during summer and autumn, respectively. Furthermore,

M_{LSC} exhibited considerable seasonal variation, as shown in Fig. 6b, with average concentrations of 33.3 and 48.6 $\mu\text{g}\cdot\text{m}^{-3}$ during summer and autumn, respectively. The seasonal variations in aerosol concentrations could be partially ascribed to the significant role of abundant summer rainfall in wet aerosol removal.

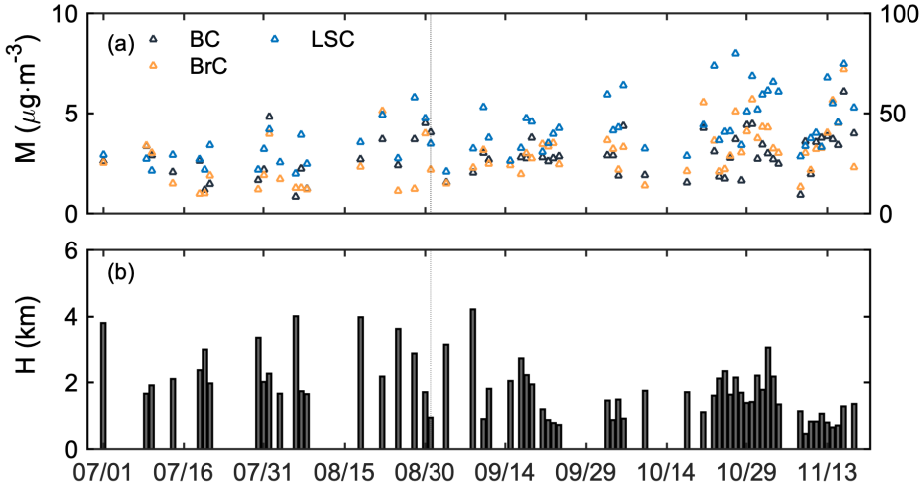


Figure 5. Aerosol optical closure results of the observation period, where (a) illustrates the mass concentrations of BrC, BC (left Y-axis) and LSC (right Y-axis); (b) illustrates the height of the aerosol diffusion boundary, and the dotted grey line represents the division between summer and autumn.

Finally, the optical properties of each aerosol species (BC, BrC, and LSC) were determined for further radiative estimations. Taking BrC as an example, the AOD (AOD_{BrC}) can be calculated using Eq. (8), and its SSA and ASY were adopted from the Mie simulation:

$$255 \quad AOD_{BrC} = H \times M_{BrC} \times MEC_{BrC}. \quad (8)$$

BC and LSC were assigned similarly to the corresponding values of AOD , SSA, and ASY. To validate the mass concentration segregation result, the calculated total aerosol scattering coefficients (Sca_{cal}) were obtained using Eq. (9) and then compared with the observed Sca (Sca_{obs}) to examine the relative errors in the concentration closure experiment. The Sca , Abs , and MSC in Eq. (9) were 525 nm:

$$260 \quad Sca_{cal} = M_{BC} \times MSC_{BC} + M_{BrC} \times MSC_{BrC} + M_{LSC} \times MSC_{LSC}. \quad (9)$$

The consistency between the Sca_{cal} and Sca_{obs} results indicated the feasibility of the optical closure study results (Fig. 6).

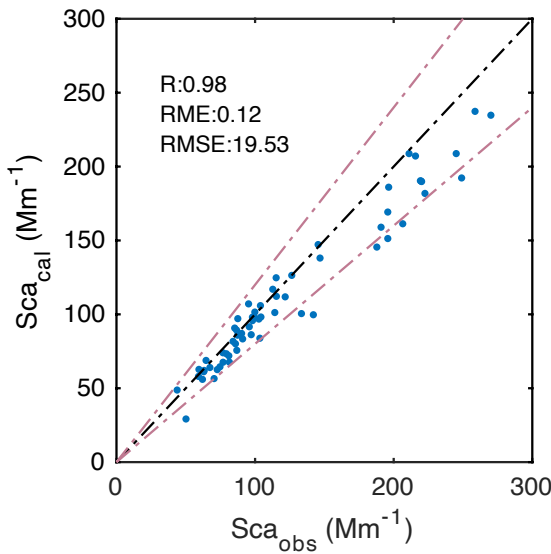


Figure 6. Comparison of observed Sca (Sca_{obs}) and calculated Sca (Sca_{cal}), the red line is the 20% relative error line.

4 BrC radiative effects

265 Based on the BrC, BC, and remaining aerosol properties from the coupling of observations and modeling, the LibRadTran was used to calculate the BrC radiative effects (Mayer and Kylling, 2005; Ma et al., 2019). LibRadTran was performed three times for aerosol scenarios with all aerosols, without BrC, and without BC, and the differences were used to determine the contributions of BrC or BC. Specifically, we used the one-dimensional discrete ordinate radiative transfer (DISORT) model as the radiative transfer solver, and the solar spectrum ranging between 300 and 2500 nm was divided into seven spectral bands 270 centered at 370, 470, 520, 590, 660, and 950 nm, following Lu et al. (2020). The average aerosol optical properties, namely AOD , SSA , and ASY of each band were obtained from our optical closure study and were used to estimate the radiative effects. The spectral surface albedo followed that in Liao et al. (1999), and a solar zenith angle of 60° was used. To examine the aerosol radiative effects, a vertical aerosol distribution must be specified to clarify the aerosol profiles (Yu et al., 2017; Lu et al., 2020). All aerosols were assumed to be uniformly distributed vertically within the aerosol diffusion height H .

275

Figure 7 shows the daily average BrC and BC RF estimations at the bottom of the atmosphere (BOA), at TOA, and in the atmosphere (AT). The RF within wavelengths 300–700 nm and 300–2500 nm are illustrated in the left and right panels, respectively. In the wavelength range 300–700 nm, the daily mean BC RF at the BOA varied from -3.9 to -36.0 W m^{-2} , with mean values of $-17.0 \pm 8.3 \text{ W m}^{-2}$, and the daily BrC RF varied from -1.5 to -15.4 W m^{-2} , with mean values of $-5.6 \pm 3.1 \text{ W m}^{-2}$. In the AT, the daily mean BC and BrC RF varied from 4.2 to 40.0 W m^{-2} and from 0.8 to 9.1 W m^{-2} , with mean values of 18.5 ± 9.2 and $3.2 \pm 1.8 \text{ W m}^{-2}$, respectively. The BC and BrC RFs at the TOA were estimated at 1.5 ± 0.9 and $-2.4 \pm 1.2 \text{ W m}^{-2}$, respectively. In the wavelength range 300–2500 nm, the daily mean BC and BrC RF at the BOA ranged from -5.8 to $-$

53.3 and from -1.8 to -18.4 W m^{-2} , respectively, with mean values of -25.2 ± 12.3 and $-6.8 \pm 3.7 \text{ W m}^{-2}$. The values in the AT ranged from 6.2 to 59.6 and from 1.0 to 11.4 W m^{-2} , respectively, with mean values of 27.6 ± 13.7 and $4.0 \pm 2.3 \text{ W m}^{-2}$. The BC and BrC RFs at the TOA were estimated at 2.4 ± 1.4 and $-2.7 \pm 1.4 \text{ W m}^{-2}$, respectively. Accordingly, the fractional BrC RF relative to BC RF (RRF) in the wavelength range 300–2500 nm at the BOA was $27.7 \pm 7.7\%$, and in the AT it was $15.0 \pm 4.2\%$. The RRF at the BOA was $34.2 \pm 9.6\%$ and in the AT it was $18.1 \pm 5.1\%$ when considering the UV–VIS range (300–700 nm). These values fall within the range of reported values in China, with the average values ranging from 15% to 26% (Huang et al., 2018; Li et al., 2020).

290

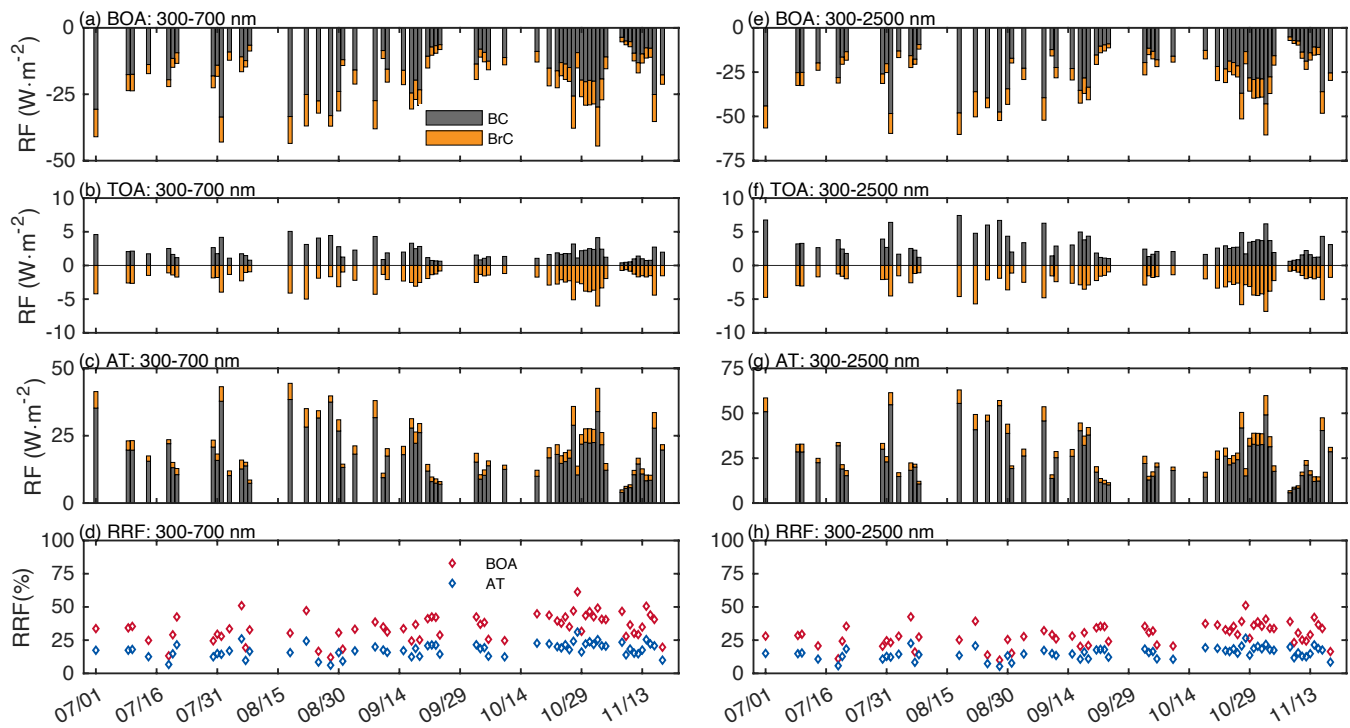


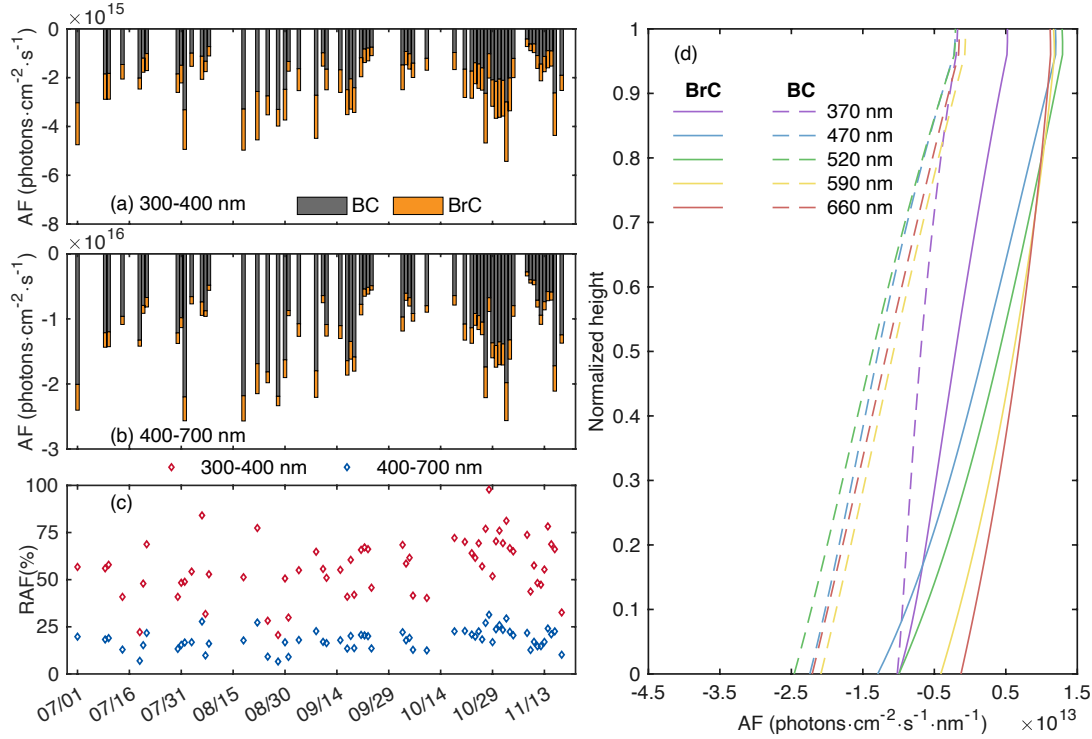
Figure 7. Daily BrC and BC RFs at the BOA, the TOA, and in the AT integrated in the wavelength range 300–700 nm are shown in (a), (b), and (c), respectively. Daily fractional BrC RF relative to BC RF (RRF) is shown in (d). Corresponding results integrated in the wavelength range 300–2500 nm are shown in (e)–(h).

295

BrC has strong absorption in the UV and shorter spectral regions, which efficiently reduce the AF and, thereby, affect atmospheric photochemistry and tropospheric ozone production (Jacobson, 1998; Mohr et al., 2013). Figure 8a and 8b show that both BC and BrC decreased the AF in the UV range (300–400 nm) and visible range (400–700 nm), consistent with the results of an investigation conducted in Guangzhou (Li et al., 2020). In the UV range, we estimated the BC-induced and BrC-induced AF at $-1.7 \times 10^{15} \pm 0.7 \times 10^{15}$ and $-9.2 \times 10^{14} \pm 4.8 \times 10^{14}$ photons $\text{s}^{-1} \text{cm}^{-2}$, respectively, and in the visible range at $-10.9 \times 10^{15} \pm 4.9 \times 10^{15}$ and $-2.0 \times 10^{15} \pm 1.2 \times 10^{15}$ photons $\text{s}^{-1} \text{cm}^{-2}$, respectively. In addition, the attenuation effects of BrC relative to that caused by BC (RAF) were significant at $57.0 \pm 15.5\%$ in the UV range and $18.4 \pm 5.3\%$ in the visible range (Fig. 8c).

These findings suggest that BrC substantially affects atmospheric photochemistry. The impacts of BrC and BC on AF were investigated on November 10, 2021, with considerable RAF in the UV (300–400 nm) and visible (400–700 nm) ranges.

305 Figure 8d shows the BrC-induced and BC-induced AF in the vertical direction, with both exhibiting decreasing trends from the surface upward. The BrC-induced AF changed from negative to positive at a certain height. The BC-induced AF was always positive from the surface upward. These differences are relevant to their differences in absorptive capacity.



310 **Figure 8. Daily average AF induced by BrC and BC (a) in the UV wavelength range (300–400 nm), and (b) in the visible wavelength range (400–700 nm). Accordingly, (c) illustrates the BrC-induced AF relative to BC-induced AF in the two wavelength ranges. (d) Vertical profile of BrC-induced and BC-induced AF at wavelengths of 370, 470, 520, 590, and 660 nm. Here, the height is normalized.**

The impact of BrC-induced AF in the UV range (300–400 nm) was more significant than that in the visible range (400–700 nm). Therefore, BrC absorption could lead to a general reduction in NO₂ photolysis rates, resulting in a maximum decrease in surface O₃ concentrations (Jo et al., 2016). This factor is particularly relevant for areas with substantial biomass burning and biofuel emissions, where BrC could significantly affect the air quality and climate. Another concern is the potential impact of BrC on the photosynthetically active radiation (PAR) used in the photosynthesis process, which refers to a spectral range of solar radiation of 400–700 nm. Figure 9 shows the PAR induced by both BrC and BC aerosol at the surface. During the 315 observation period, the direct attenuation of PAR induced by BrC and BC was estimated at -4.9 ± 2.7 and $-15.1 \pm 7.4 \text{ W m}^{-2}$, respectively, which slowed down plant photosynthesis rates and reduced vegetation productivity. Figure 9b shows the

proportion of PAR induced by BrC relative to that induced by BC (RPAR), with an average and standard deviation value of $33.5 \pm 9.4\%$. These findings highlight the significant impact of BrC on vegetation and its potential role in the environment.

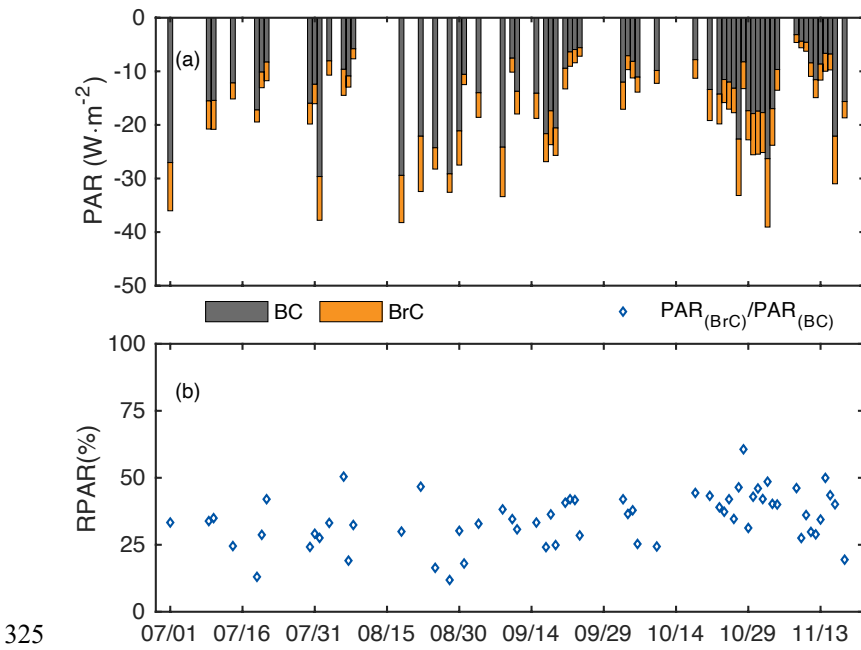


Figure 9. Daily average (a) BrC-induced PAR and BC-induced PAR, and (b) fractional BrC-induced PAR relative to BC-induced PAR.

Based on the daily results for RRF, RAF, and RPAR, we investigated their corresponding monthly averages at the BOA 330 (Fig. 10), finding that RAF is higher than other ratios. In addition, RRF, RAF, and RPAR were somewhat larger in autumn than in summer, related to the seasonal differences in BrC absorption and aerosol diffusion height.

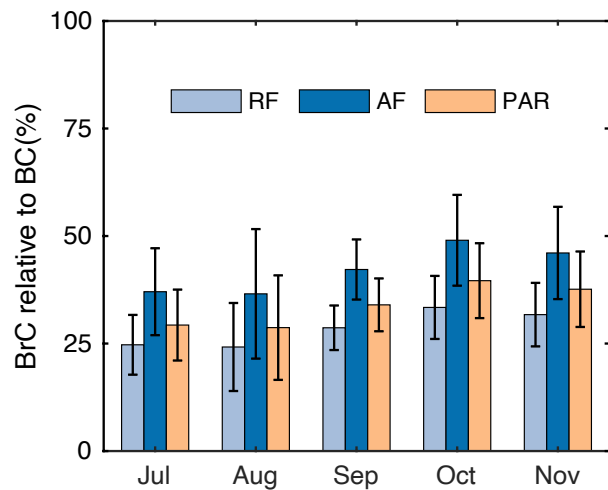


Figure 10. BrC radiative effects relative to those of BC. RF results are integrated in the wavelength range 300–2500 nm, and the AF results are integrated in the wavelength range 300–400 nm.

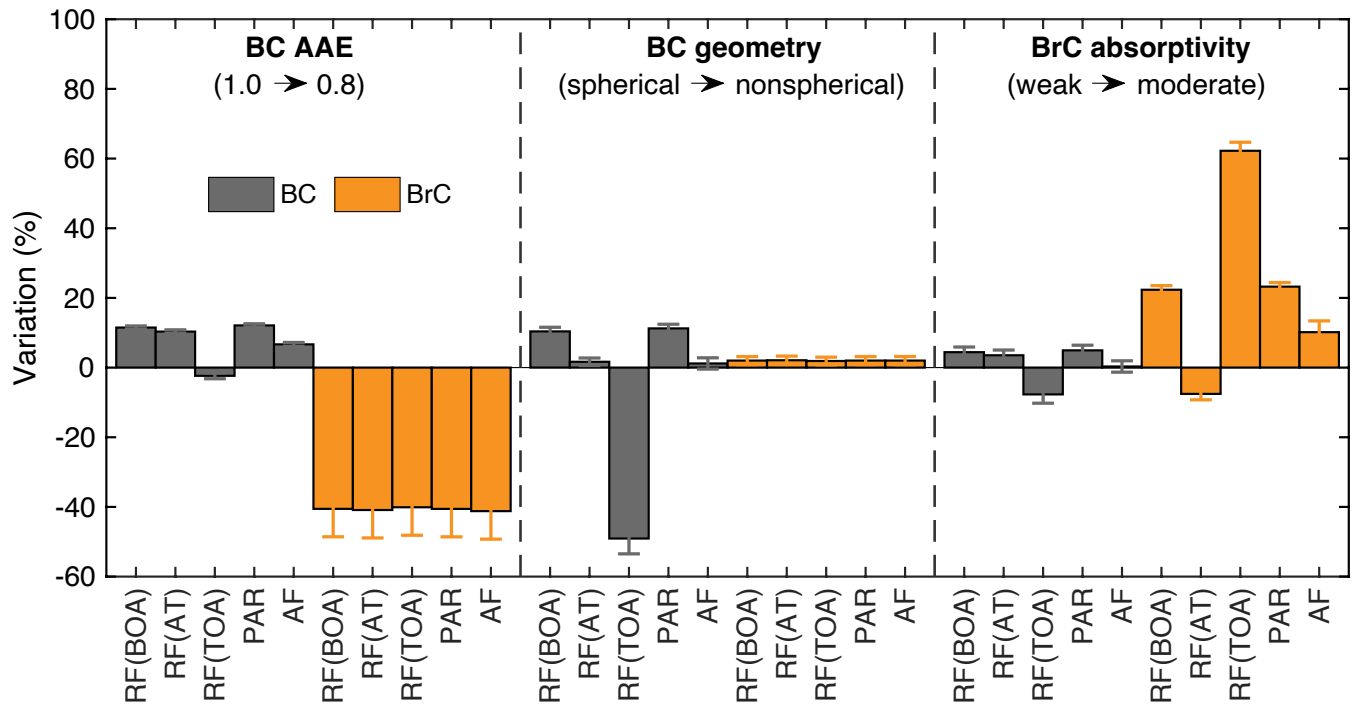
335 **5 Discussion**

As discussed above, numerous assumptions and simplifications of BC and BrC were made to segregate their radiative indices, and several major uncertain factors were considered for further investigation. For example, the assumption of $AAE_{BC} = 1$ was challenged because of BC complex microphysical properties (Liu et al., 2018), and could directly influence the segregation of BrC. We assumed that all aerosol components were homogeneous spherical, whereas BC particles are widely known to have complex chain-like aggregation structures. Further, as shown in Fig. 4, BrC imaginary parts of refractive indices k_{BrC} showed variations over an order of magnitude, which could clearly influence its optical properties. Therefore, the three factors were taken as an example to investigate their influences on estimations of BrC radiative effects. It should be noted that numerous other variables with uncertainties to different degrees, such as aerosol mixing states (internal or external mixing), vertical distributions, and the like were not discussed in this study.

345

Figure 11 shows the differences of BC and BrC radiative effects caused by the three factors, i.e., BC AAE (from the original 1.0 to the current 0.8), BC particle geometries (from the original sphere to fractal aggregate), and BrC absorptivity (from relatively weak to moderate absorption). The bars in the figure indicate corresponding relative changes compared with the results of our default setups. For BC AAE, a relatively smaller AAE_{BC} of 0.8 was selected for correspondence between the BC 350 value and the size distribution considered in our study (Liu et al., 2018). For BC particle non-sphericity, the fractal aggregate was a widely used numerical model, whereas the calculation of optical properties was significantly more challenging. We considered the optical properties of aggregates with a fractal dimension of 1.8 from the existing database developed by Liu et al. (2019). For uncertainties regarding BrC absorptivity, we considered a group of BrC refractive indices with slightly stronger absorptivity, reported by Kirchstetter et al. (2004). For all three examples, only the aforementioned factors were changed for 355 estimations of radiative effects, and all other assumptions and procedures remained the same. The BC AAE assumption showed influences on BC radiative effects with relative differences of approximately 10%, but much stronger influences on BrC radiative effects, i.e., ~40%. This result was ascribed to smaller BC AAE causing weaker BC absorption in shorter wavelengths, leading to smaller radiative effects. However, larger BrC absorption coefficients and amounts during the segregation could cause larger BrC radiative effects. The assumption regarding BC spherical particles showed minor influences on BrC radiative 360 effects, with the relative differences being less than 5%, but much stronger influences on BC radiative effects, particularly on the RF(TOA) with an average deviation of almost 50%, caused mainly by weaker scattering owing to BC non-sphericity (Li et al., 2016). In other words, the assumption regarding spherical BC led to overestimation of BC scattering, increasing the upward radiation reaching the TOA. However, the influence of BC non-sphericity on BrC/BC segregation was lower and the BrC radiative effects change was less than 5%. The right panel shows the influences deriving from uncertainties of the

365 absorptivity of BrC. Except the RF (TOA) with a relatively larger difference of 62%, the rest of the BrC radiative effects (average absolute values) were all below 30%, and, as expected, all the differences were close to zero.



370 **Figure11.** Relative variations of BC (charcoal grey bar) and BrC (orange bar) radiative effects caused by changes in their microphysical or optical properties. Three independent changes (listed in the top of this panel) are made with respect to BC AAE, BC particle geometries, and BrC absorptivity, and the bars indicate the corresponding relative changes compared with the results with our detailed setups.

6 Conclusions and future work

375 In this study, we proposed an observation-constrained and efficient approach for estimating BrC radiative effects. A state-of-the-art combination of measurements and numerical models provided primary variables for radiative transfer simulations to estimate BrC radiative effects. The light-absorbing properties of BrC obtained from aethalometer measurements and an optical separation method were combined with the simulated BrC optical properties to determine the mass concentrations. Optical closure was performed to obtain the concentrations and optical information for BrC, BC, and non-absorbing aerosol. The *AOD* and mass concentration of PM_{10} were used to constrain the total and other aerosol contents. Subsequently, radiative transfer simulations were employed to estimate BrC radiative effects, and observations over four months in Nanjing were used as an example to quantify the radiative effects of BrC. During the observational period, the absorption of BrC and BC at 370 nm 380 was in the same order of magnitude, and the ratios ranged from 8.7% to 34.1%, aligning with values reported in previous studies. The BrC-induced instantaneous RF accounted for approximately $27.7 \pm 7.7\%$ of that caused by BC at the surface and

15.0 ± 4.2% in the atmosphere. The strong absorption of BrC in the near-ultraviolet and visible regions significantly weakened
385 the PAR and AF at the surface, underscoring its non-negligible contribution to the climate. These findings provide valuable insights for understanding BrC radiative effects and indicate the importance and necessity of improving the observation and modeling of BrC properties.

Overall, this study explored an observation-constrained and efficient approach to quantify BrC radiative effects. To derive a
390 more general algorithm, we strove to segregate the BrC component by employing existing/general observations and assumptions; however, significant room for improvement of the method remains. For example, new species based on more chemical observations could be considered to increase the extinction closure of particulate matter. Further, significant uncertainties remain for aerosol mixing states and vertical distributions.

395 **Author contribution**

Jiandong Wang and Chao Liu designed and directed the study. Yueyue Cheng contributed to data analysis and wrote the first draft of this paper. Zhouyang Zhang and Li Chen helped proofread the grammar of the article. Jiaping Wang, Dafeng Ge, Caijun Zhu and Jinbo Wang collected data. Jiandong Wang, Jiaping Wang, Chao Liu and Aijun Ding contributed the data interpretation and review of the paper.

400

Competing interests

The authors declared that they have no conflict of interest.

Acknowledgements

405 This work was supported by National Key R&D Program of China (2022YFC3701000, Task 5, Jiandong Wang), and the National Natural Science Foundation of China, 42075098 (Jiandong Wang) and 42005082 (Jiaping Wang).

References

Alexander, D. T. L., Crozier, P. A., and Anderson, J. R.: Brown Carbon Spheres in East Asian Outflow and Their Optical Properties, *Science*, 321, 833–836, <https://doi.org/10.1126/science.1155296>, 2008.

410 Andreae, M. O. and Gelencser, A.: Black carbon or brown carbon? The nature of light-absorbing carbonaceous aerosols, *Atmos. Chem. Phys.*, 2006.

Arnott, W. P., Hamasha, K., Moosmüller, H., Sheridan, P. J., and Ogren, J. A.: Towards Aerosol Light-Absorption Measurements with a 7-Wavelength Aethalometer: Evaluation with a Photoacoustic Instrument and 3-Wavelength
415 Nephelometer, *Aerosol Sci. Technol.*, 39, 17–29, <https://doi.org/10.1080/027868290901972>, 2005.

Barnard, J. C., Volkamer, R., and Kassianov, E. I.: Estimation of the mass absorption cross section of the organic carbon component of aerosols in the Mexico City Metropolitan Area, *Atmos. Chem. Phys.*, 8, 6665–6679, <https://doi.org/10.5194/acp-8-6665-2008>, 2008.

Bond, T. C., Habib, G., and Bergstrom, R. W.: Limitations in the enhancement of visible light absorption due to mixing state, 420 *J. Geophys. Res.-Atmos.*, 111, D20211, <https://doi.org/10.1029/2006JD007315>, 2006.

Bond, T. C., Doherty, S. J., Fahey, D. W., Forster, P. M., Berntsen, T., DeAngelo, B. J., Flanner, M. G., Ghan, S., Kärcher, B., Koch, D., Kinne, S., Kondo, Y., Quinn, P. K., Sarofim, M. C., Schultz, M. G., Schulz, M., Venkataraman, C., Zhang, H., Zhang, S., Bellouin, N., Guttikunda, S. K., Hopke, P. K., Jacobson, M. Z., Kaiser, J. W., Klimont, Z., Lohmann, U., Schwarz, J. P., Shindell, D., Storelvmo, T., Warren, S. G., and Zender, C. S.: Bounding the role of black carbon in the climate system: 425 A scientific assessment: BLACK CARBON IN THE CLIMATE SYSTEM, *J. Geophys. Res.-Atmos.*, 118, 5380–5552, <https://doi.org/10.1002/jgrd.50171>, 2013.

Cai, J., Zeng, X., Zhi, G., Gligorovski, S., Sheng, G., Yu, Z., Wang, X., and Peng, P.: Molecular composition and photochemical evolution of water-soluble organic carbon (WSOC) extracted from field biomass burning aerosols using high-resolution mass spectrometry, *Atmos. Chem. Phys.*, 20, 6115–6128, <https://doi.org/10.5194/acp-20-6115-2020>, 2020.

430 Chakrabarty, R. K., Moosmüller, H., Chen, L.-W. A., Lewis, K., Arnott, W. P., Mazzoleni, C., Dubey, M. K., Wold, C. E., Hao, W. M., and Kreidenweis, S. M.: Brown carbon in tar balls from smoldering biomass combustion, *Atmos. Chem. Phys.*, 10, 6363–6370, <https://doi.org/10.5194/acp-10-6363-2010>, 2010.

Chen, P., Kang, S., Tripathee, L., Ram, K., Rupakheti, M., Panday, A. K., Zhang, Q., Guo, J., Wang, X., Pu, T., and Li, C.: Light absorption properties of elemental carbon (EC) and water-soluble brown carbon (WS-BrC) in the Kathmandu Valley, 435 Nepal: A 5-year study, *Environ. Pollut.*, 261, 114239, <https://doi.org/10.1016/j.envpol.2020.114239>, 2020.

Chen, Y. and Bond, T. C.: Light absorption by organic carbon from wood combustion, *Atmos. Chem. Phys.*, 2010.

Cheng, Y., He, K., Du, Z., Engling, G., Liu, J., Ma, Y., Zheng, M., and Weber, R. J.: The characteristics of brown carbon aerosol during winter in Beijing, *Atmos. Environ.*, 127, 355–364, <https://doi.org/10.1016/j.atmosenv.2015.12.035>, 2016.

Cheng, Y. F., Eichler, H., Wiedensohler, A., Heintzenberg, J., Zhang, Y. H., Hu, M., Herrmann, H., Zeng, L. M., Liu, S., 440 Gnauk, T., Brüggemann, E., and He, L. Y.: Mixing state of elemental carbon and non-light-absorbing aerosol components derived from in situ particle optical properties at Xinken in Pearl River Delta of China, *J. Geophys. Res.-Atmos.*, 111, D20204, <https://doi.org/10.1029/2005JD006929>, 2006.

Choudhary, V., Singh, G. K., Gupta, T., and Paul, D.: Absorption and radiative characteristics of brown carbon aerosols during crop residue burning in the source region of Indo-Gangetic Plain, *Atmos. Res.*, 249, 105285, 445 <https://doi.org/10.1016/j.atmosres.2020.105285>, 2021.

Coen, M. C., Weingartner, E., Apituley, A., Ceburnis, D., Fierz-Schmidhauser, R., Flentje, H., Henzing, J. S., Jennings, S. G., Moerman, M., Petzold, A., Schmid, O., and Baltensperger, U.: Minimizing light absorption measurement artifacts of the Aethalometer: evaluation of five correction algorithms, *Atmos. Meas. Tech.*, 2010.

450 Ding, A. J., Fu, C. B., Yang, X. Q., Sun, J. N., Zheng, L. F., Xie, Y. N., Herrmann, E., Nie, W., Petäjä, T., Kerminen, V.-M., and Kulmala, M.: Ozone and fine particle in the western Yangtze River Delta: an overview of 1 yr data at the SORPES station, *Atmos. Chem. Phys.*, 13, 5813–5830, <https://doi.org/10.5194/acp-13-5813-2013>, 2013.

Ding, A., Nie, W., Huang, X., Chi, X., Sun, J., Kerminen, V.-M., Xu, Z., Guo, W., Petäjä, T., Yang, X., Kulmala, M., and Fu, C.: Long-term observation of air pollution-weather/climate interactions at the SORPES station: a review and outlook, *Front. Environ. Sci. En.*, 10, 15, <https://doi.org/10.1007/s11783-016-0877-3>, 2016.

455 Du, Z., He, K., Cheng, Y., Duan, F., Ma, Y., Liu, J., Zhang, X., Zheng, M., and Weber, R.: A yearlong study of water-soluble organic carbon in Beijing II: Light absorption properties, *Atmos. Environ.*, 89, 235–241, <https://doi.org/10.1016/j.atmosenv.2014.02.022>, 2014.

Feng, Y., Ramanathan, V., and Kotamarthi, V. R.: Brown carbon: a significant atmospheric absorber of solar radiation?, *Atmos. Chem. Phys.*, 13, 8607–8621, <https://doi.org/10.5194/acp-13-8607-2013>, 2013.

460 Feng, W., Shao, Z. J., Wang, Q. G., Xie, M. J.: Size-resolved light-absorbing organic carbon and organic molecular markers in Nanjing, east China: Seasonal variations and sources. *Environ. Pollut.*, 332, 122006, <https://doi.org/10.1016/j.envpol.2023.122006>, 2023.

Hoffer, A., Tóth, A., Nyirő-Kósa, I., Pósfai, M., and Gelencsér, A.: Light absorption properties of laboratory-generated tar ball particles, *Atmos. Chem. Phys.*, 16, 239–246, <https://doi.org/10.5194/acp-16-239-2016>, 2016.

465 Huang, R.-J., Yang, L., Cao, J., Chen, Y., Chen, Q., Li, Y., Duan, J., Zhu, C., Dai, W., Wang, K., Lin, C., Ni, H., Corbin, J. C., Wu, Y., Zhang, R., Tie, X., Hoffmann, T., O'Dowd, C., and Dusek, U.: Brown Carbon Aerosol in Urban Xi'an, Northwest China: The Composition and Light Absorption Properties, *Environ. Sci. Technol.*, 52, 6825–6833, <https://doi.org/10.1021/acs.est.8b02386>, 2018.

Jacobson, M. Z.: Studying the effects of aerosols on vertical photolysis rate coefficient and temperature profiles over an urban airshed, *J. Geophys. Res.-Atmos.*, 103, 10593–10604, <https://doi.org/10.1029/98JD00287>, 1998.

470 Jo, D. S., Park, R. J., Lee, S., Kim, S.-W., and Zhang, X.: A global simulation of brown carbon: implications for photochemistry and direct radiative effect, *Atmos. Chem. Phys.*, 16, 3413–3432, <https://doi.org/10.5194/acp-16-3413-2016>, 2016.

Kaskaoutis, D. G., Grivas, G., Stavroulas, I., Bougiatioti, A., Liakakou, E., Dumka, U. C., Gerasopoulos, E., and Mihalopoulos, N.: Apportionment of black and brown carbon spectral absorption sources in the urban environment of Athens, Greece, during 475 winter, *Sci. Total Environ.*, 801, 149739, <https://doi.org/10.1016/j.scitotenv.2021.149739>, 2021.

Kirchstetter, T. W. and Thatcher, T. L.: Contribution of organic carbon to wood smoke particulate matter absorption of solar radiation, *Atmos. Chem. Phys.*, 12, 6067–6072, <https://doi.org/10.5194/acp-12-6067-2012>, 2012.

Kirchstetter, T. W., Novakov, T., and Hobbs, P. V.: Evidence that the spectral dependence of light absorption by aerosols is affected by organic carbon, *J. Geophys. Res.-Atmos.*, 109, D21208, <https://doi.org/10.1029/2004JD004999>, 2004.

480 Kirillova, E. N., Andersson, A., Tiwari, S., Srivastava, A. K., Bisht, D. S., and Gustafsson, Ö.: Water-soluble organic carbon aerosols during a full New Delhi winter: Isotope-based source apportionment and optical properties: WSOC aerosols during a New Delhi winter, *J. Geophys. Res.-Atmos.*, 119, 3476–3485, <https://doi.org/10.1002/2013JD020041>, 2014.

485 Lack, D. A. and Cappa, C. D.: Impact of brown and clear carbon on light absorption enhancement, single scatter albedo and absorption wavelength dependence of black carbon, *Atmos. Chem. Phys.*, 10, 4207–4220, <https://doi.org/10.5194/acp-10-4207-2010>, 2010.

Lack, D. A. and Langridge, J. M.: On the attribution of black and brown carbon light absorption using the Ångström exponent, *Atmos. Chem. Phys.*, 13, 10535–10543, <https://doi.org/10.5194/acp-13-10535-2013>, 2013.

Laskin, A., Laskin, J., and Nizkorodov, S. A.: Chemistry of Atmospheric Brown Carbon, *Chem. Rev.*, 115, 4335–4382, <https://doi.org/10.1021/cr5006167>, 2015.

490 Li, J., Liu, C., Yin, Y., and Kumar, K. R.: Numerical investigation on the Ångström exponent of black carbon aerosol, *J. Geophys. Res. Atmos.*, 121, 3506–3518, doi:10.1002/2015JD024718, 2016.

Li, J., Zhang, Q., Wang, G., Li, J., Wu, C., Liu, L., Wang, J., Jiang, W., Li, L., Ho, K. F., and Cao, J.: Optical properties and molecular compositions of water-soluble and water-insoluble brown carbon (BrC) aerosols in northwest China, *Atmos. Chem. Phys.*, 20, 4889–4904, <https://doi.org/10.5194/acp-20-4889-2020>, 2020.

495 Liakakou, E., Kaskaoutis, D. G., Grivas, G., Stavroulas, I., Tsagkaraki, M., Paraskevopoulou, D., Bougiatioti, A., Dumka, U. C., Gerasopoulos, E., and Mihalopoulos, N.: Long-term brown carbon spectral characteristics in a Mediterranean city (Athens), *Sci. Total Environ.*, 708, 135019, <https://doi.org/10.1016/j.scitotenv.2019.135019>, 2020.

Liao, H., Yung, Y. L., and Seinfeld, J. H.: Effects of aerosols on tropospheric photolysis rates in clear and cloudy atmospheres, *J. Geophys. Res.-Atmos.*, 104, 23697–23707, <https://doi.org/10.1029/1999JD900409>, 1999.

500 Lin, G., Penner, J. E., Flanner, M. G., Sillman, S., Xu, L., and Zhou, C.: Radiative forcing of organic aerosol in the atmosphere and on snow: Effects of SOA and brown carbon, *J. Geophys. Res.-Atmos.*, 119, 7453–7476, <https://doi.org/10.1002/2013JD021186>, 2014.

Liu, C., Chung, C. E., Zhang, F., and Yin, Y.: The colors of biomass burning aerosols in the atmosphere, *Sci. Rep.*, 6, 28267, <https://doi.org/10.1038/srep28267>, 2016.

505 Liu, C., Chung, C. E., Yin, Y., Schnaiter, M.: The absorption Ångström° exponent of black carbon: from numerical aspects, *Atmos. Chem. Phys.*, 18, 6259–6273, <https://doi.org/10.5194/acp-18-6259-2018>, 2018.

Liu, C., Xu, X., Yin, Y., Schnaiter, M., and Yung, Y. L.: Black carbon aggregates: A database for optical properties, *J. Quant. Spectrosc. Radiat. Transf.*, 222–223, 170–179, <https://doi.org/10.1016/j.jqsrt.2018.10.021>, 2019.

Liu, J., Scheuer, E., Dibb, J., Ziembka, L. D., Thornhill, Kenneth. L., Anderson, B. E., Wisthaler, A., Mikoviny, T., Devi, J. J., 510 Bergin, M., and Weber, R. J.: Brown carbon in the continental troposphere, *Geophys. Res. Lett.*, 41, 2191–2195, <https://doi.org/10.1002/2013GL058976>, 2014.

Liu, X., Zhang, Y.-L., Peng, Y., Xu, L., Zhu, C., Cao, F., Zhai, X., Haque, M. M., Yang, C., Chang, Y., Huang, T., Xu, Z., Zhang, W., Fan, M., and Lee, X.: Chemical and optical properties of carbonaceous aerosols in Nanjing, eastern China: regionally transported biomass burning contribution, *Atmos. Chem. Phys.*, 19, 11213–11233, <https://doi.org/10.5194/acp-19-11213-2019>, 2019.

Lu, Q., Liu, C., Zhao, D., Zeng, C., Li, J., Lu, C., Wang, J., and Zhu, B.: Atmospheric heating rate due to black carbon aerosols: Uncertainties and impact factors, *Atmos. Res.*, 240, 104891, <https://doi.org/10.1016/j.atmosres.2020.104891>, 2020.

Lu, Z., Streets, D., Winijkul, E., Yan, F., Chen, Y., Bond, T., Feng, Y., Dubey, M., Liu, S., Pinto, J., and Carmichael, G.: Light absorption properties and radiative effects of primary organic aerosol emissions., *Environ. Sci. Technol.*, 49, 4868–4877, <https://doi.org/10.1021/acs.est.5b00211>, 2015.

520 Ma, N., Zhao, C. S., Nowak, A., Müller, T., Pfeifer, S., Cheng, Y. F., Deng, Z. Z., Liu, P. F., Xu, W. Y., Ran, L., Yan, P., Göbel, T., Hallbauer, E., Mildenberger, K., Henning, S., Yu, J., Chen, L. L., Zhou, X. J., Stratmann, F., and Wiedensohler, A.: Aerosol optical properties in the North China Plain during HaChi campaign: an in-situ optical closure study, *Atmos. Chem. Phys.*, 11, 5959–5973, <https://doi.org/10.5194/acp-11-5959-2011>, 2011.

525 Ma, Y., Zhang, M., Jin, S., Gong, W., Chen, N., Chen, Z., Jin, Y., and Shi, Y.: Long-Term Investigation of Aerosol Optical and Radiative Characteristics in a Typical Megacity of Central China During Winter Haze Periods, *J. Geophys. Res.-Atmos.*, 124, 12093–12106, <https://doi.org/10.1029/2019JD030840>, 2019.

Mayer, B. and Kylling, A.: Technical note: The libRadtran software package for radiative transfer calculations – description and examples of use, *Atmos. Chem. Phys.*, 5, 1855–1877, <https://doi.org/10.5194/acp-5-1855-2005>, 2005.

530 Mohr, C., Lopez-Hilfiker, F. D., Zotter, P., Prevot, A. S. H., Xu, L., Ng, N. L., Herndon, S. C., Williams, L. R., Franklin, J. P., Zahniser, M. S., Worsnop, D. R., Knighton, W. B., Aiken, A. C., Gorkowski, K. J., Dubey, M. K., Allan, J. D., and Thornton, J. A.: Contribution of Nitrated Phenols to Wood Burning Brown Carbon Light Absorption in Detling, United Kingdom during Winter Time, *Environ. Sci. Technol.*, 47, 6316–6324, <https://doi.org/10.1021/es400683v>, 2013.

Moosmüller, H., Chakrabarty, R. K., Ehlers, K. M., and Arnott, W. P.: Absorption Ångström coefficient, brown carbon, and 535 aerosols: basic concepts, bulk matter, and spherical particles, *Atmos. Chem. Phys.*, 11, 1217–1225, <https://doi.org/10.5194/acp-11-1217-2011>, 2011.

Pani, S. K., Lin, N.-H., Griffith, S. M., Chantara, S., Lee, C.-T., Thepnuan, D., and Tsai, Y., I.: Brown carbon light absorption over an urban environment in northern peninsular Southeast Asia, *Environ. Pollut.*, 276, 116735, <https://doi.org/10.1016/j.envpol.2021.116735>, 2021.

540 Paraskevopoulou, D., Kaskaoutis, D. G., Grivas, G., Bikkina, S., Tsagkaraki, M., Vrettou, I. M., Tavernaraki, K., Papoutsidaki, K., Stavroulas, I., Liakakou, E., Bougiatioti, A., Oikonomou, K., Gerasopoulos, E., and Mihalopoulos, N.: Brown carbon absorption and radiative effects under intense residential wood burning conditions in Southeastern Europe: New insights into the abundance and absorptivity of methanol-soluble organic aerosols, *Sci. Total Environ.*, 860, 160434, <https://doi.org/10.1016/j.scitotenv.2022.160434>, 2023.

545 Saleh, R.: From Measurements to Models: Toward Accurate Representation of Brown Carbon in Climate Calculations, *Curr. Pollut. Rep.*, 6, 90–104, <https://doi.org/10.1007/s40726-020-00139-3>, 2020.

Saleh, R., Marks, M., Heo, J., Adams, P. J., Donahue, N. M., and Robinson, A. L.: Contribution of brown carbon and lensing to the direct radiative effect of carbonaceous aerosols from biomass and biofuel burning emissions, *J. Geophys. Res.-Atmos.*, 120, 10285–10296, <https://doi.org/10.1002/2015JD023697>, 2015.

550 Schmid, O., Artaxo, P., Arnott, W. P., Chand, D., Gatti, L. V., Frank, G. P., Hoffer, A., Schnaiter, M., and Andreae, M. O.: Spectral light absorption by ambient aerosols influenced by biomass burning in the Amazon Basin. I: Comparison and field calibration of absorption measurement techniques, *Atmos. Chem. Phys.*, 6, 3443–3462, <https://doi.org/10.5194/acp-6-3443-2006>, 2006.

Shamjad, P. M., Tripathi, S. N., Thamban, N. M., and Vreeland, H.: Refractive Index and Absorption Attribution of Highly 555 Absorbing Brown Carbon Aerosols from an Urban Indian City-Kanpur, *Sci. Rep.*, 6, 37735, <https://doi.org/10.1038/srep37735>, 2016.

Shen, Z., Lei, Y., Zhang, L., Zhang, Q., Zeng, Y., Tao, J., Zhu, C., Cao, J., Xu, H., and Liu, S.: Methanol Extracted Brown Carbon in PM2.5 Over Xi'an, China: Seasonal Variation of Optical Properties and Sources Identification, *Aerosol Sci. Eng.*, 1, 57–65, <https://doi.org/10.1007/s41810-017-0007-z>, 2017.

560 Virkkula, A., Chi, X., Ding, A., Shen, Y., Nie, W., Qi, X., Zheng, L., Huang, X., Xie, Y., Wang, J., Petäjä, T., and Kulmala, M.: On the interpretation of the loading correction of the aethalometer, *Atmos. Meas. Tech.*, 8, 4415–4427, <https://doi.org/10.5194/amt-8-4415-2015>, 2015.

Wang, X., Heald, C. L., Ridley, D. A., Schwarz, J. P., Spackman, J. R., Perring, A. E., Coe, H., Liu, D., and Clarke, A. D.: Exploiting simultaneous observational constraints on mass and absorption to estimate the global direct radiative forcing of 565 black carbon and brown carbon, *Atmos. Chem. Phys.*, 14, 10989–11010, <https://doi.org/10.5194/acp-14-10989-2014>, 2014.

Wang, X., Heald, C. L., Sedlacek, A. J., de Sá, S. S., Martin, S. T., Alexander, M. L., Watson, T. B., Aiken, A. C., Springston, S. R., and Artaxo, P.: Deriving brown carbon from multiwavelength absorption measurements: method and application to AERONET and Aethalometer observations, *Atmos. Chem. Phys.*, 16, 12733–12752, <https://doi.org/10.5194/acp-16-12733-2016>, 2016.

570 Wang, J., Nie, W., Cheng, Y., Shen, Y., Chi, X., Wang, J., Huang, X., Xie, Y., Sun, P., Xu, Z., Qi, X., Su, H., and Ding, A.: Light absorption of brown carbon in eastern China based on 3-year multi-wavelength aerosol optical property observations and an improved absorption Ångström exponent segregation method, *Atmos. Chem. Phys.*, 18, 9061–9074, <https://doi.org/10.5194/acp-18-9061-2018>, 2018a.

Wang, Y., Ma, P.-L., Peng, J., Zhang, R., Jiang, J. H., Easter, R. C., and Yung, Y. L.: Constraining Aging Processes of Black 575 Carbon in the Community Atmosphere Model Using Environmental Chamber Measurements, *J. Adv. Model. Earth Sy.*, 10, 2514–2526, <https://doi.org/10.1029/2018MS001387>, 2018b.

Yan, C., Zheng, M., Sullivan, A. P., Bosch, C., Desyaterik, Y., Andersson, A., Li, X., Guo, X., Zhou, T., Gustafsson, Ö., and Collett, J. L.: Chemical characteristics and light-absorbing property of water-soluble organic carbon in Beijing: Biomass burning contributions, *Atmos. Environ.*, 121, 4–12, <https://doi.org/10.1016/j.atmosenv.2015.05.005>, 2015.

580 Yan, J., Wang, X., Gong, P., Wang, C., and Cong, Z.: Review of brown carbon aerosols: Recent progress and perspectives, *Sci. Total Environ.*, 634, 1475–1485, <https://doi.org/10.1016/j.scitotenv.2018.04.083>, 2018.

Yang, M., Howell, S. G., Zhuang, J., and Huebert, B. J.: Attribution of aerosol light absorption to black carbon, brown carbon, and dust in China – interpretations of atmospheric measurements during EAST-AIRE, *Atmos. Chem. Phys.*, 9, 2035–2050, <https://doi.org/10.5194/acp-9-2035-2009>, 2009.

585 Yu, X., Lü, R., Liu, C., Yuan, L., Shao, Y., Zhu, B., and Lei, L.: Seasonal variation of columnar aerosol optical properties and radiative forcing over Beijing, China, *Atmos. Environ.*, 166, 340–350, <https://doi.org/10.1016/j.atmosenv.2017.07.011>, 2017.

Yuan, J.-F., Huang, X.-F., Cao, L.-M., Cui, J., Zhu, Q., Huang, C.-N., Lan, Z.-J., and He, L.-Y.: Light absorption of brown carbon aerosol in the PRD region of China, *Atmos. Chem. Phys.*, 16, 1433–1443, <https://doi.org/10.5194/acp-16-1433-2016>, 2016a.

590 Yuan, L., Yin, Y., Xiao, H., Yu, X., Hao, J., Chen, K., and Liu, C.: A closure study of aerosol optical properties at a regional background mountainous site in Eastern China, *Sci. Total Environ.*, 550, 950–960, <https://doi.org/10.1016/j.scitotenv.2016.01.205>, 2016b.

Zeng, L. H., Zhang, A. X., Wang, Y. H., Wagner, N. L., Katich, J. M., Schwarz, J. P., Schill, G. P., Brock, C., Froyd, K. D., Murphy, D. M., Williamson, C. J., Kupc, A., Scheuer, E., Dibb, J., and Weber, R. J.: Global measurements of brown carbon and estimated direct radiative effects, *Geophys. Res. Lett.*, 47, e2020GL088747, <https://doi.org/10.1029/2020GL088747>, 2020.

595 Zhang, L., Sun, J. Y., Shen, X. J., Zhang, Y. M., Che, H., Ma, Q. L., Zhang, Y. W., Zhang, X. Y., and Ogren, J. A.: Observations of relative humidity effects on aerosol light scattering in the Yangtze River Delta of China, *Atmos. Chem. Phys.*, 15, 8439–8454, <https://doi.org/10.5194/acp-15-8439-2015>, 2015.

Zhang, Y., Ma, Y., and Gong, W.: Retrieval of Brown Carbon based on the aerosol complex refractive indices in the winter of 600 Wuhan, *Geo-Spat. Inf. Sci.*, 20, 319–324, <https://doi.org/10.1080/10095020.2017.1394660>, 2017a.

Zhang, Y., Forrister, H., Liu, J., Dibb, J., Anderson, B., Schwarz, J. P., Perring, A. E., Jimenez, J. L., Campuzano-Jost, P., Wang, Y., Nenes, A., and Weber, R. J.: Top-of-atmosphere radiative forcing affected by brown carbon in the upper troposphere, *Nat. Geosci.*, 10, 486–489, <https://doi.org/10.1038/ngeo2960>, 2017b.

605 Zhang, A., Wang, Y., Zhang, Y., Weber, R. J., Song, Y., Ke, Z., and Zou, Y.: Modeling the global radiative effect of brown carbon: a potentially larger heating source in the tropical free troposphere than black carbon, *Atmos. Chem. Phys.*, 20, 1901–1920, <https://doi.org/10.5194/acp-20-1901-2020>, 2020.

Zhang, W., Wang, W., Li, J., Ma, S., Lian, C., Li, K., Shi, B., Liu, M., Li, Y., Wang, Q., Sun, Y., Tong, S., and Ge, M.: Light absorption properties and potential sources of brown carbon in Fenwei Plain during winter 2018-2019, *J. Environ. Sci.*, 102, 53–63, <https://doi.org/10.1016/j.jes.2020.09.007>, 2021a.

610 Zhang, Y., Peng, Y., Song, W., Zhang, Y.-L., Ponsawansong, P., Prapamontol, T., and Wang, Y.: Contribution of brown carbon to the light absorption and radiative effect of carbonaceous aerosols from biomass burning emissions in Chiang Mai, Thailand, *Atmos. Environ.*, 260, 118544, <https://doi.org/10.1016/j.atmosenv.2021.118544>, 2021b.

Zhong, M. and Jang, M.: Dynamic light absorption of biomass-burning organic carbon photochemically aged under natural sunlight, *Atmos. Chem. Phys.*, 14, 1517–1525, <https://doi.org/10.5194/acp-14-1517-2014>, 2014.

615 Zhu, C.-S., Qu, Y., Zhou, Y., Huang, H., Liu, H.-K., Yang, L., Wang, Q.-Y., Hansen, A. D. A., and Cao, J.-J.: High light
absorption and radiative forcing contributions of primary brown carbon and black carbon to urban aerosol, GONDWANA
Res., 90, 159–164, <https://doi.org/10.1016/j.gr.2020.10.016>, 2021.